(2)

SECOND ANNUAL TECHNICAL REPORT

on

ONR Grant No: N00014-90-J-4039

(July 1, 1991 to June 30, 1992)

by

Dr. Chen S. Tsai

Professor and Principal Investigator

Department of Electrical and Computer Engineering

and

Institute for Surface and Interface Science

University of California, Irvine

Irvine, California 92717

Magnetostatic Waves-Based Integrated Optic Bragg Cell Modules

With Applications To RF Signal Processing

(ONR Grant No.: N00014-90-J-4039)

2nd ~~First~~ Annual Technical Report

Dr. Chen S. Tsai

Principal Investigator

SUMMARY OF PROGRESS

Two major achievements were made during the second program year (July 1, 1991 to June 30, 1992): First, a complete analysis on guided-wave magnetooptic (MO) Bragg diffraction in a YIG-GGG layer structure aimed at the key parameters and guidelines for design of high-performance MO Bragg cells has been carried out. Second, an integrated MO Bragg cell module has been realized, for the first time, using a YIG-GGG tapered waveguide structure.

I. INTRODUCTION AND OBJECTIVE

Although Magneto-optics in waveguide structures [1] was among the areas actively pursued during the early phase of Guided-Wave Optics research, research activity in this area was greatly reduced between the mid 70's and early 80's. However, a revival of interest in this area has taken place recently. One subject of this renewed interest concerns collinear [2] and noncollinear (transverse Bragg) [3] magnetooptic (MO) interactions between guided-optical waves (GOW) and magnetostatic waves (MSW) in Yttrium Iron Garnet-Gadolinium Gallium Garnet (YIG-GGG) waveguides. MSWs are slow-propagating electromagnetic waves which result from propagation of electron spin precession around a DC magnetic field in a thin film of ferromagnetic

material such as YIG on a suitable substrate such as GGG. MSWs have their energy confined in a small depth beneath the ferromagnetic film, and can be readily and efficiently generated by applying a microwave signal to a short-circuited metallic strip brought into close proximity. The center frequency of the MSWs can be tuned, typically form 1.0 to higher than 20 GHz simply by varying the DC magnetic field. Guided-wave MO interactions result from the moving optical grating induced by the MSW through the Faraday and Cotton-Mouton effects, similar to a guide-wave acoustooptic (AO) interaction [4] in which the surface acoustic wave (SAW) induces a moving optical grating through the photoelastic effect. The periodicity of the resulting optical grating is determined by the dispersive relation between the velocity and the frequency of the MSW as function of the DC magnetic field. In a noncollinear [3] coplanar geometry as shown in Fig.1, a portion of an incident light is Bragg diffracted and mode-converted as a result. The resulting MO Bragg modulators are called MO Bragg cells [5] in analogy with the prevalent AO Bragg cells.

In comparison to their AO counterparts, the unique advantages associated with the MO Bragg cells are: 1. A much larger range of tunable carrier frequencies may by obtained by varying the DC magnetic field [6]. Such high and tunable carrier frequencies with the MO devices allows direct processing at the carrier frequency of wideband RF signals and eliminated the need for indirect processing via frequency down-conversion as is required with the AO devices; 2. A large MO bandwidth may be realized by means of a simpler transducer [5]; and 3. Much higher and electronically tunable modulation/switching and scanning speeds are achievable as the velocity of propagation for the MSWs can be higher than that of the SAWs by one- to two- orders of magnitude [7].

The objective of this ONR-sponsored research is to explore the potential of the magnetostatic waves-based integrated MO Bragg cell modules for applications in real-time processing of wideband RF signals at microwave carrier frequencies.

II. MAJOR PROGRESS

During the second program year two major advances were made: 1. A complete analysis on guided-wave magnetooptic (MO) Bragg diffraction in a YIG-GGG layer structure aimed at the key parameters and guidelines for design of high-performance MO Bragg cells has been carried out. 2. An integrated MO Bragg cell module has been realized, for the first time, using a YIG-GGG tapered waveguide structure. A detail report on each now follows.

A. GUIDED-WAVE MAGNETOOPTIC BRAGG DIFFRACTION FROM MAGNETOSTATIC FORWARD VOLUME WAVES

In this section, we present findings of a recent study [8] on excitation and propagation of magnetostatic forward volume waves (MSFVW) and related MO Bragg diffraction in a layer structure which consists of ferromagnetic YIG film, GGG substrate, lift-off space between transducer and YIG film surface, and two ground planes of finite separation as shown in Fig.1. A homogeneous DC magnetic field is applied perpendicularly to the YIG-GGG waveguide in order to facilitate excitation and propagation of the MSFVW by a microstrip line transducer [9,10]. For simplicity the thickness of the transducer strip is ignored in this analysis.

A1. RF Magnetization of the MSFVW

Although the general configuration of Fig.1 had been utilized for construction of a variety of MSW devices [11,12], no report of any specific expression for the RF magnetization of the MSFVW has appeared in the literature heretofore. We have most recently carried out an analysis [8] to arrive at an explicit expression for the RF magnetization. Here we shall summarize the results obtained, but leave the detailed calculations to the reference [8]. The MSFVW is to propagate in the Y-direction and the

incident light wave of TE-mode in the X-direction. The boundary-value problem involved is analyzed by simultaneously satisfying the Maxwell's equations and the gyromagnetic equation together withy appropriate boundary conditions.

We shall now express the X- and Y- components of the RF magnetization in terms of magnetostatic wave power (P_{MSFVW}) and RF drive power (P_0) as follows:

$$|m_x| = \frac{2\kappa\left(1 + e^{-2|K|\ell}\right)|K|\,Q(K,z)}{\beta\sqrt{\omega\mu_0 C}}\sqrt{\frac{P_{MSFVW}}{L}} \tag{1a}$$

$$|m_y| = \left(\frac{\omega_0}{\omega}\right)|m_x| \tag{1b}$$

where L is the aperture of the transducer, μ_0 is the permeability of free space, $\omega_0 = \gamma H_i$ is the ferromagnetic resonance frequency in which γ designates the gyromagnetic ratio and H_i the internal magnetic field, and C and Q(K,z) are complex functions of geometrical parameters and the wave vector and frequency K and ω. Explicit expression are given in Ref. [8]. Also, μ and κ are the diagonal and the off-diagonal components of the relative permeability tensor [μ] associated with the MSW, $\beta \equiv \sqrt{-\mu}$, and ℓ is the thickness of the GGG substrate.

Finally, the RF magnetization with propagation loss taken into account are expressed in terms of the RF drive power as follows:

$$|m_x| = 2\kappa\frac{\left(1 + e^{-2|K|\ell}\right)|K|\,Q(K,z)\,e^{\mathrm{Im}(\kappa)\,D}\,e^{0.115\,IL}}{\beta\sqrt{\omega\mu_0 C}}\sqrt{\frac{P_0}{L}} \tag{2a}$$

$$|m_y| = \left(\frac{\omega_0}{\omega}\right)|m_x| \tag{2b}$$

where the relationship among the one way RF-MSFVW coupling loss (IL), the input RF drive power (P_0), and the magnetostatic wave power (P_{MSFVW}) is given as follows:

$$P_{MSFVW} = P_0\, 10^{IL/10} \cong P_0\, e^{0.230\, IL} \tag{2c}$$

and D denotes the distance between the transducer strip and the position of interest along the propagation path of the MSFVW.

A2. MO Bragg Diffraction or Mode-Conversion Efficiency vs Drive Powers

Based on an earlier analysis using coupled-mode theory [13], the MO Bragg diffraction or mode-conversion (TE to TM mode and vice versa) efficiency is given as follows:

$$\eta^{\pm} = \frac{(\kappa^{\pm})^2}{(\kappa^{\pm})^2 + (\Delta/2)^2} \sin^2\left[\sqrt{(\kappa^{\pm})^2 + (\Delta/2)^2}\, L\right] \tag{3}$$

where $\Delta \equiv |\vec{\beta}_{TE} - \vec{\beta}_{TM} \pm \vec{K}|$ is the phase mismatch among the three wave vectors $\vec{\beta}_{TE}$ (undiffracted wave), $\vec{\beta}_{TM}$ (diffracted wave) and $\vec{K}$ (MSFVW) and L is the interaction length or the aperture of the MSFVW involved. The coupling coefficient $\kappa^{\pm}$ takes the following form when the spatial distribution of $|m_x|$ and $|m_y|$ are assumed to be uniform in Z-direction and the optical wave is well confined in the waveguide [13]:

$$\kappa^{\pm} \equiv \kappa_1 \pm \kappa_2 \tag{4a}$$

$$\kappa_1 \equiv \frac{-k_0\, |m_x|}{4\sqrt{\varepsilon_r}} f_1 \tag{4b}$$

$$\kappa_2 \equiv \frac{k_0\, |m_y|\, M_s}{4\sqrt{\varepsilon_r}} \left(2f_{44} + \frac{2}{3}\Delta f\right) \tag{4c}$$

$$\Delta f \equiv f_{11} - f_{12} - 2f_{44} \tag{4d}$$

where k_0 is the propagation constant of the guided-light in free space, ε_r is the relative dielectric constant of the waveguide at the optical wavelength involved, f_1 is the first-order magnetic birefringence (Faraday Effect), and f_{11}, f_{12}, and f_{44} are the three independent components of the second-order magnetic birefringence (Cotton-Mouton Effect). Note that the term Δf includes the contribution of the Cotton-Mouton effect [3,13,14,15]. The signs of "+" and "−" designate the situations for Anti-Stokes (with the frequency of the diffracted light up-shifted) and Stokes (with the frequency of the diffracted light down-shifted) interactions [6,13,15], respectively. Note that the phases of m_y and m_x, associated with Faraday and Cotton-Mouton effects, have been incorporated in Eqs.(4b) and (4c). These phases result in the Anti-Stokes and Stokes interactions as indicated by the sign "±". Finally, note that the superscripts ± and the subscripts 1 and 2 are added to κ to differentiate them from the off-diagonal component of the permeability tensor. For the situation with perfect phase-matching ($\Delta \equiv 0$), Eq.(3) leads to the following form:

$$\eta^{\pm} = \sin^2\left\{ \frac{k_0}{4\sqrt{\varepsilon_r}} \left[-f_1 |m_x| \pm \left(2 f_{44} + \frac{2}{3} \Delta f \right) |m_y| \right] L \right\} \tag{5}$$

Using the simple relation between $|m_x|$ and $|m_y|$ given in Eq.(1b), the diffraction efficiency $\eta^{\pm}$ can be expressed in terms of $|m_x|$ alone.

Finally, by substituting Eqs.(1a) and (2a) into Eq.(5) the explicit relationship between the diffraction efficiency $\eta^{\pm}$ and the drive powers P_{MSFVW} and P_0 are obtained as follows:

$$\eta^{\pm} = \sin^2\left[\mathcal{S} \left(M_F \pm \frac{\omega_0}{\omega} M_{CM} \right) \sqrt{P_{MSFVW}\, L} \right] \tag{6}$$

and

$$\eta^{\pm} = \sin^2\left[\mathcal{S}\left(M_F \pm \frac{\omega_0}{\omega} M_{CM} \right) e^{\mathrm{Im}(\kappa)\, D}\, e^{0.115\, IL} \sqrt{P_0\, L} \right] \tag{7}$$

where

$$\mathcal{S} \equiv \frac{2\pi \times 10^{-3}\, \kappa \left(1 + e^{-2|K| l} \right) |K|\, Q(K,z)}{\beta \sqrt{\omega\, \mu_0\, C}} \tag{8a}$$

$$M_F \equiv \frac{-k_0\, f_1}{\sqrt{\varepsilon_r}} \tag{8b}$$

$$M_{CM} \equiv \frac{-k_0}{\sqrt{\varepsilon_r}} \left(2\, f_{44} + \frac{2}{3} \Delta f \right) \tag{8c}$$

Note that $\mathcal{S}$ is a function of the DC magnetic field H_0, the carrier frequency of the MSFVW (ω) and the corresponding wave vector ($\vec{K}$), and the geometrical parameters of the layered structure. Since the data of magnetic parameters is usually given in the Gaussian unit system, the unit for MSFVW magnetization must be converted form the MKSA unit system to the Gaussian unit system in Eq.(5). For this reason a factor $2\pi \times 10^{-3}$ is added in Eq.(8a). The Gaussian unit system is used in the numerical calculation that has been carried out. M_F and M_{CM} are the terms related to the MO properties of the ferromagnetic material. The subscripts F and CM designate, respectively, the Faraday and Cotton-Mouton effects. Since M_F and M_{CM} are the only material-related terms, they may be used as figures of merit for the guided-wave MO Bragg devices. Alternatively, $\mathcal{S}M_F$ and $\mathcal{S}M_{CM}$ may be used as the effective MO figure of merits. The two terms, $e^{\,0.115\, IL}$ and $e^{\mathrm{Im}(\kappa)\, D}$ in Eq.(7) represent, respectively, the

coupling loss of the transducer and the propagation loss of the MSFVW. Comparing Eqs.(6) and (7) to the corresponding expressions for AO or EO interaction [4] we see that the only difference lies in the term S. It is this term that provides freedom for optimizing the MO interaction and the performance of the resulting MO devices. For example, the effects of the DC magnetic field on the tunability of the operating carrier frequency and the effects of the DC magnetic field and the thickness of the YIG film on other major device performances are found to be sensitive functions of this term.

A3. Sample Numerical Results

Using the analytical results presented in subsections A1 and A2 and Ref.[8], various device performances such as carrier frequency and MO Bragg bandwidth as well as diffraction efficiency can be calculated using electronic computers. The diffraction efficiency η is found to be proportional to the square of the linear combination of the RF magnetizations $|m_x|$ and $|m_y|$ when the product of $\kappa^{\pm}$ and L varies in the lower region of $[0,\pi/2]$. For the Bismuth-doped YIG waveguide [16,17], we have $\sqrt{\varepsilon_r}=2.4$ at the optical wavelength (λ_0) of 1.3 μm, saturation magnetization $4\pi M_s=1800$ Oe, and f_1, f_{44} and Δf are 2.22×10^{-6} Oe^{-1}, 3.70×10^{-11} Oe^{-2}, and 1.85×10^{-11} Oe^{-2}, respectively [5,6,18]. Using these published data we have generated the plots for η as a function of $|m_x|$ and $|m_y|$ with the MO interaction length of 1.5, 1.0 and 0.5 centimeters given in Fig.2. For example, for Anti-Stokes interaction [13] with 1.0 cm interaction length 50 and 100% diffraction efficiencies are predicted when the magnetization $|m_x|$ approaches 70 and 130 Oe, respectively. As an example, at a DC magnetic field of 5180 Oe 100% diffraction efficiency at the optical wavelength of 1.3 μm can be obtained from a Bragg Cell with a 3.0 μm thick layer of presently available Bi-doped YIG film using the microstrip line transducer with an interaction length of 1.0 cm and a strip width of 15 μm at the MSFVW power of 20 mW/mm. The corresponding center carrier frequency and 3 dB bandwidth of the first passband are, respectively, 10 GHz and 900 MHz. Note that the

magnitude of the RF magnetization $|m_x|$ or $|m_y|$ is proportional to the square root of the RF drive power density (P_0/L) (see Eq.(2)). Therefore at a constant drive power density, and thus a constant RF magnetization, the diffraction efficiency will be proportional to the square of the interaction length L (see Eq.(5)). From Eq.(7), however, it can be seen that at a constant total RF drive power (P_0), the diffraction efficiency will be proportional to L. This conclusion is valid for a sufficiently small value for the product of κ and L. Otherwise, the exact sinsoidal variation should be used. In the numerical calculation, we set a constant RF drive power density so that the resulting diffraction efficiency η for the interaction lengths of 1.5, 1.0 and 0.5 cm can be read directly from Fig.2 once the magnitudes of the RF magnetization are known. It also can be seen from Fig.2 that to obtain the same diffraction efficiency the corresponding total RF drive power for the first two interaction lengths will be, respectively, nine and four times the total RF drive power for the third. Finally, note that in Ref.[8] the RF magnetization $|m_x|$ was analyzed separately with respect to the carrier frequency at constant total RF drive power P_0 and total MSFVW power P_{MSFVW}, DC magnetic field H_0, and geometrical parameters d,g,t,ℓ etc.

REFERENCES

[1] See for example, P. K. Tien, R. J. Martin, R. Wolf, R. C. LeCraw, and S. L. Black,"Switching and modulation of light in magneto-optic waveguides of garnet films," Appl. Phys. Lett., Vol.21, pp.394-396, 1972.

[2] A.D. Fisher, J.N. Lee, E.S. Gaynor, and A.B. Tveten, "Optical Guided-Wave Interaction with Magnetostatic Waves at Microwave Frequency," Appl. Phys. Lett., Vol.41, pp.779-781, 1982.

[3] (a) C.S. Tsai,"Hybrid Integrated Optic Modules for Real-Time Signal Processing," Proc. of NASA Optical Information Processing Conference II, NASA Conference Publication No. 2302, pp.149-164, 1983.

(b) C.S. Tsai, D.Young, W. Chen, L. Adkins, C.C. Lee, and H. Glass, "Noncollinear Coplanar Magneto-Optic Interaction of Guided Optical Waves and Magnetostatic Surface Waves in Yittrium Iron Garnet-Gadolinium Gallium Garnet Waveguide," Appl. Phys. Lett., Vol.47, pp.651-654, 1985.

[4] C.S. Tsai, "Guided-wave Acoustooptic Bragg Modulators for Wide-Band Integrated Optic Communications and Signal Processing," IEEE Trans. on Circuits and System, vol.CAS-26, pp.1072-1098, Dec. 1979.

[5] D. Young and C.S. Tsai, "GHz Bandwidth Magneto-Optic Interaction in Yittrium Iron Garnet-Gadolinium Gallium Garnet Using Magnetostatic Forward Volume Waves," Appl. Phys. Lett. Vol.53, pp.1696-1698, 1988.

[6] D. Young and C.S. Tsai, "X-band Magneto-optic Bragg Cell Using Bismuth-Doped Yittrium Iron Garnet Waveguide," Appl. Phys. Lett., Vol.54, pp.2242-2244, 1989.

[7] C.S. Tsai and D. Young, "Wideband Scanning of a Guided-Light Beam and Spectrum Analysis Using Magnetostatic Waves in an Yittrium Iron Garnet-Gadolinium Gallium Garnet Waveguide," Appl. Phys. Lett., Vol.54, pp.196-198, 1989.

[8] Y. Pu and C.S. Tsai,"RF Magnetization of Magnetostatic Forward Volume Wave in a YIG-GGG Layer Structure with Application to Design of High-Performance Guided-Wave Magnetooptic Bragg Cells," International Journal of High Speed Electronics, Vol.2, pp.185-208, 1991.

[9] (a) See, for example, R.W. Damon and J.R. Eshbach, "Magnetostatic Modes of a Ferromagnetic Slab," J.Phys. Chem. Solids, Vol.19, pp.308-320, 1961.

(b)R. W. Damon and H. Van De Vaart, "Propagation of Magnetostatic Spin Waves at Microwave Frequencies in a Normally-Magnetized Disk," J. Appl. Phys., Vol.36, pp.3453-3459, 1965.

[10](a)A.G. Ganguly and D.C. Webb, "Microstrip Excitation of Magnetostatic Surface Waves: Theory and Experiment," IEEE Trans. Microwave Theory Technology, Vol.MTT-23, pp.998-1006, 1975.

(b)See, for example, I.J. Weinberg and J.C.Sethares, "Magnetostatic Volume Wave," 1983 IEEE MTT-DIGEST, pp.253-255, 1983.

[11]W. S. Ishak, "Magnetostatic Wave Technology: A review," Proc. IEEE, Vol.76, pp.171-187, 1988.

[12](a) J.D. Adam and J.H. Collins,"Microwave Magnetostatic Delay Devices Based on Epitaxial Yttrium Iron Garnet," Proc. IEEE., Vol.64, pp.794-800, 1976.

(b) J. D. Adam, "Analog Signal Processing with Microwave Magnetics," Proc. IEEE, Vol.76, pp.159-170, 1988.

[13]C. S. Tsai and D. Young,"Magnetostatic-Forward-Volume-Wave-Based Guided-Wave Magneto-Optic Bragg Cells and Applications to Communications and Signal Processing," IEEE Trans. on Microwave Theory and Technology., Vol.MTT-38, pp.560-570, 1990.

[14](a) Yu. V. Gulyaev, I.A. Ignat'ev, V.G. Plekhanov, and A.F. Popkov,"Waveguide Propagation of Light in a Ferrimagnetic Film Containing a Magnetostatic Wave," Sov. Phys. Solid State, Vol.27, pp.845-847, 1985.

(b) O. G. Rutkin et al., " Interaction of Optical Waveguide Modes with Spin Waves in an Yttrium Iron Garnet Film," Sov. Tech. Phys. Lett., Vol.11, pp.386-387, 1985.

(c) A. A. Solomko. Yu. A. Gaidai, A. V. Dovzhenko, M. V. Antonishin, and A. T. Yanishevskii, "Collinear Interaction of Light with Surface Magnetostatic Waves in Ferrite-Garnet Films," Opt. Spectrosc. (USSR), Vol.61, pp.804-807, 1986.

(d) A. D. Boardman, Yu. V. Gulyaev, and S. A. Nikitov,"Thin-Film solid State Devices Based on Nonlinear Magnetostatic Waves," Japanese Jour. Appl. Phys., Vol.27, pp. L2438-2441, 1988.

[15] A.N. Sigaev and A.A. Stashkevich,"Anisotropic Diffraction of Optical Waveguide Modes by a Bulk Spin Wave in an Yttrium Iron Garnet Film," Sov. Tech. Phys. Lett., Vol.14, pp.209-210, 1988.

[16] (a) K. Ando, N. Takeda, T. Okuda, and N. Koshizuka, "Waveguide Mode Conversion by Magnetic Linear Birefringence of Bi-substituted Iron Garnet Films Tilted from (111)," J. Appl. Phys., Vol.57, pp.718-722, 1985.

(b)N. Koshizuka, K. Ando, and T. Okuda, "Growth-Induced Birefringence in LPE-grown Iron Garnet Films," in Proc. Int. Symp. Magneto-Optics, J. Magn. Soc. Jpn., Vol.11S, pp.281-286, 1987.

[17] (a) H. LeGall, M. Guillot, A. Marcnand, Y. Nomi, and M. Artinian,"Faraday Rotation in Bismuth Substituted Iron Garnets," Proc. Int. Symp. Magneto-Optics, J. Magn. Soc. Jpn., Vol.11S, pp.235-240, Apr. 1987.

(b) J.P. Krumme, V. Doormann, and R. Eckart,"Bismuth-Substituted Iron Garnet Films Prepared by RF Diode Sputtering," IEEE Trans. Magn., Vol.MAG-20, pp.983-985, Sept. 1984.

(c) H. Kenz, P. Hansen,m and W. Tolksdorf, " Growth-Induced Magnetic and Optic Anisotropy in Bismuth-Substituted Iron Garnet Films," Appl. Phys. Letts., Vol.54, pp.2484-2486, 1989.

[18] P.V. Pisarev, I.G. Sinii, N.N. Kolpalova, and Yu. M. Yakovlev, "Magnetic Birefringence of Light in Iron Garnets," Sov. Phys. JETP., Vol.33, pp.1175-1182, 1971.

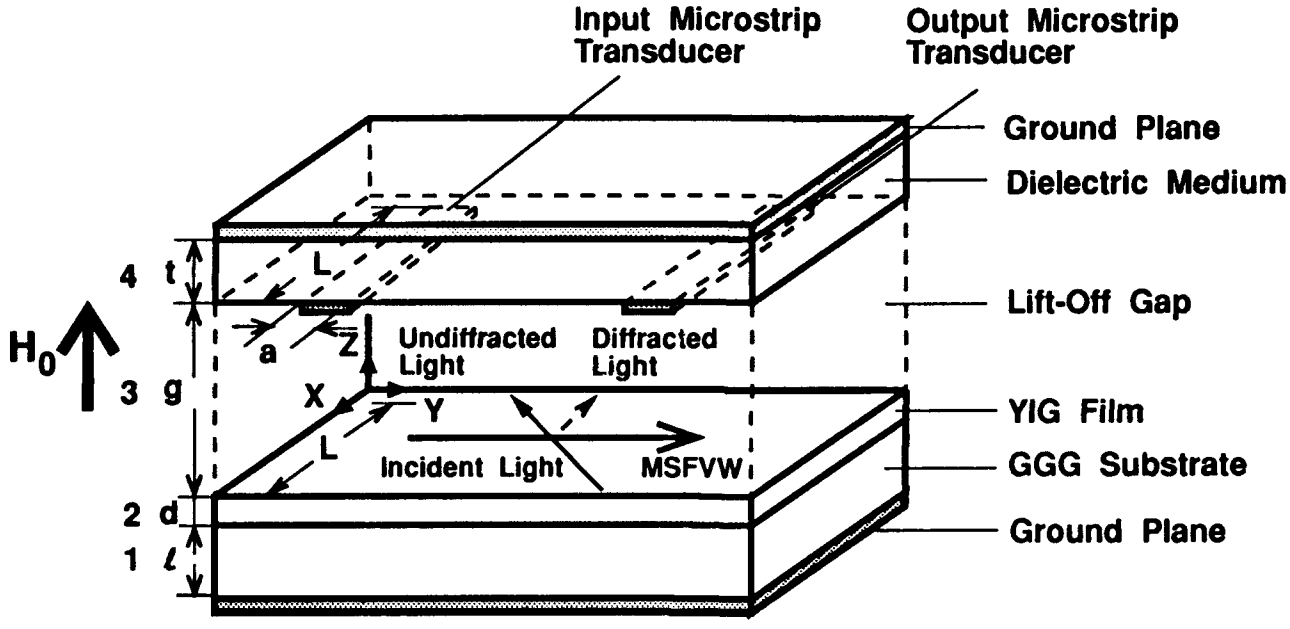

Fig.1 The YIG-GGG Layered Structure for MSFVW and Guided-Wave Magnetooptic Bragg Diffraction

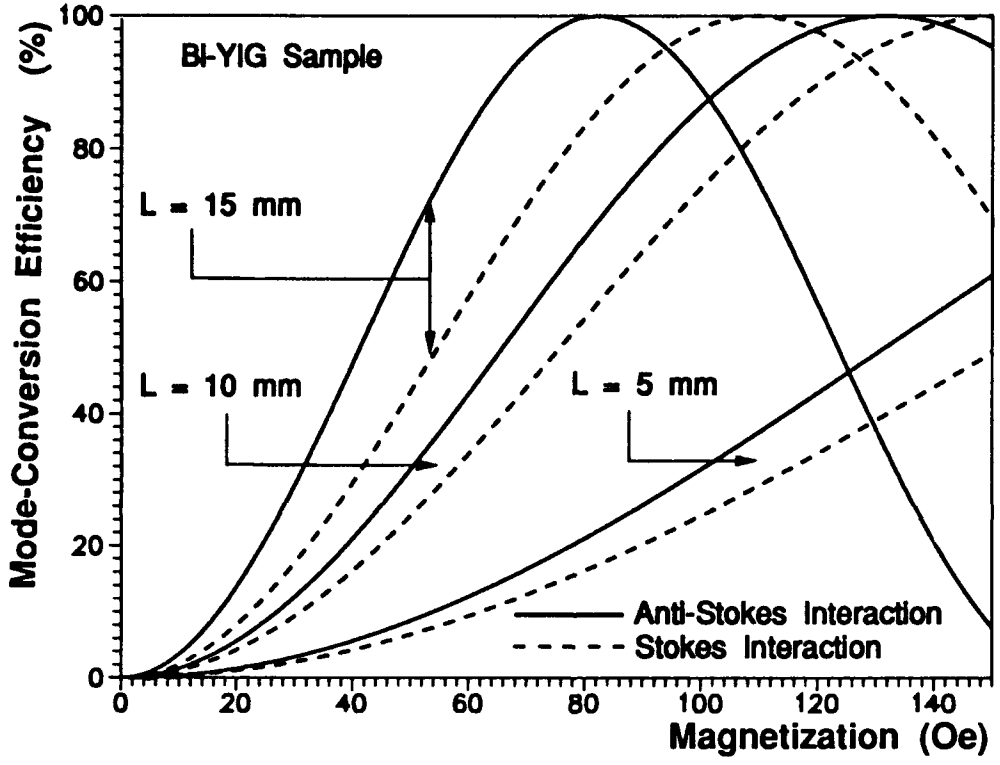

Fig.2 Mode-Conversion (Bragg Diffraction) Efficiency of Guided-Wave Magnetooptic Bragg Diffraction Versus RF Magnetization of the MSFVW

B. INTEGRATED MAGNETOOPTIC BRAGG CELL MODULES IN YIG-GGG TAPER WAVEGUIDE

Magnetostatic waves (MSWs)-based guided-wave magnetooptic (MO) Bragg cells in yttrium iron garnet-gadolinium gallium garnet (YIG-GGG) waveguides[1] possess the unique capabilities of electronically tunable carrier frequency and GHz bandwidth, and are, therefore, capable of performing direct RF signal processing at the carrier frequencies from 0.5 to far beyond X-band[2]-[4]. Other capabilities include multiport optical deflection and switching at a speed one- to three-order of magnitude higher than that of AO Bragg cells[2]. Thus, recent realization of high-performance guided-wave MO Bragg cells and demonstration of the aforementioned applications have motivated our interest toward realization of integrated MO Bragg cell modules in which waveguide lenses and lens arrays are integrated with the MO Bragg cell in the same YIG-GGG substrate.

Negative-index change hybrid waveguide lenses which combine analog Fresnel and chirp gratings were fabricated recently in GaAs, $LiNbO_3$ and YIG-GGG waveguide substrates using ion-milling technique[5]-[7]. It has been concluded that the thinner the waveguide, the smaller the required milled-depth in the gratings in order to produce desired index changes, and thus ensures high lens throughput. It has also been shown recently that the MO bandwidth is approximately proportional to the thickness of the YIG waveguide[8]. Therefore, there exists contradictory requirements on the waveguide thickness for achieving both wideband MO interaction and high lens throughput. In this paper, we report a tapered YIG-GGG waveguide structure to accommodate simultaneously the requirements for large MO Bragg bandwidth and high lens throughput, and thus enables the realization of high-performance integrated MO Bragg cell modules. The experimental results of newly devised curved hybrid lenses configured in the two side regions of the waveguide of smaller thickness are first presented. The

design of the MO Bragg cell fabricated in the central region of the waveguide of larger thickness and the results of MO experiments with the resulting integrated MO Bragg cell module are then presented and discussed.

We had reported previously the construction of flat hybrid lenses on YIG-GGG waveguide using the ion-milling technique[6]. Such ion-milled lenses had provided both high efficiency and near diffraction-limited focal spot size for a light beam propagating within a small angle from the lens axis. However, the overall lens performance was significantly degraded due to the high degree of coma incurred when the light beam propagated at a larger angle from the lens axis. We have realized a newly devised curved hybrid lens in which the hybrid lens lies on a contour g(z) rather than a straight line to greatly reduce the coma[9] (Fig.1).

The integrated MO Bragg cell module was constructed in a tapered Bi-doped YIG-GGG waveguide 6.0×16.0 mm^2 in size. As shown in the middle region of Fig.2, the initial thickness of the YIG waveguide layer was 3.25 μm. The two end regions of the tapered waveguide was ion-milled down to 2.68 μm in several steps in order to produce a gradual transition, and thus ensure a high transmission for the light beam. The curved hybrid lenses[10] with 4.0 mm focal length and 0.8 mm aperture were then fabricated onto the two end regions using ion-milling technique. Measurements on the lenses were carried out using a 1.3 μm diode laser and prism-coupling of TE_0-mode in the waveguide. The focused light beam was coupled out of the polished edge of the waveguide and imaged upon a beamscan system for measurement. Figs.3a and 3b show the focal spot profiles obtained from the curved hybrid lenses at 0 and ±3.5 degree from the lens axis, respectively. It shows practically no coma with sidelobe levels lower than 12.3 dB from the main lobe. The measured -3dB focal spot size and throughput efficiency were 3.52 μm and 27.6 %, respectively, as compared to the calculated diffraction-limited spot size of 2.44 μm and calculated throughput efficiency of 80 %. The focused spot profile of the lens pair (Fig.3c) shows a measured -3 dB focal spot size

of 6.26 μm. The calculated efficiency, however, has not taken into account the optical loss caused by insufficient resolution of the photolithography in the Fresnel zone portion of the hybrid lens. Also due to the small index change (0.004), the thickness (300 μm) of the hybrid lens became longer in order to have the required phase change and therefore caused more fabrication losses. Thus, the discrepancy between the measured and calculated diffraction efficiencies is believed to be caused by the relatively low resolution of 1.0 μm used in our photolithography system and the non-perfect lens pattern produced by ion-milling. The total acceptance angle of the lens (defined as the total off-axis angular span in which the efficiency of the lens stays more than 50% of the on-axis efficiency) was measured to be 7 degrees. The lenses were found to be practically coma-free up to this angular field of view.

An MO Bragg cell was subsequently formed by incorporating a microstrip line transducer in the middle region of the tapered waveguide. The middle section of the waveguide was set at 6.0 mm in order to enable usage of Bragg interaction length up to 5.0 mm, where the microstrip line transducers were placed. In this particular design, the transducer had a strip width of 60 μm and a length of 5.0 mm which was also the MO interaction length. The two end regions were 5.0 mm each in order to accommodate the thickness and the focal length of the lens. A compact magnetic housing[11] was used to provide the required DC magnetic field for saturation of the YIG layer and excitation of tunable wideband magnetostatic forward volume waves (MSFVWs). Again, the 1.3 μm laser diode was used to measure the performances of the resulting integrated MO Bragg cell module.

Fig.4 is the photograph of scanned and focused diffracted light spots taken at the output edge of the waveguide as the carrier frequency of the RF drive signal was varied from 7.35 to 7.65 GHz and 10.25 to 10.75 GHz at DC magnetic fields of 2820 and 3700 Oe, respectively. Also shown is the focused undiffracted light spot. It is clear that the

curved hybrid lens pair has successfully facilitated collimation and focusing of the light beam required in an integrated MO Bragg cell module.

The bandwidth of the MO Bragg cell module was measured to be 260 MHz at the center carrier frequency of 9970 MHz and a DC magnetic field of 3600 Oe. The calculated bandwidths for the YIG layer thickness of 3.25 and 2.68 μm are 300 and 250 MHz, respectively. The good agreement obtained confirms the capability of the tapered waveguide structure to preserve the MO interaction bandwidth. The single-frequency resolution[12] is determined by

$$\Delta f = \left(\frac{0.88 \times V_{msw}}{d}\right) \times \frac{1}{\left\{1 - \frac{f}{V_{msw}} \times \frac{dV_{msw}}{df}\right\}}$$

in which V_{msw} and f designate, respectively, the velocity and the carrier frequency of the MSFVW and d the optical beam width. It is seen that due to the dispersive nature of the MSW the frequency resolution depends upon the carrier frequency. The measured frequency resolution was 35 MHz as compared to the calculated resolution of 25 MHz at the center carrier frequency of 10.30 GHz. The diffraction efficiency of the module was measured to be 2.0 % at the carrier frequency of 9990 MHz and the RF drive power of 31.2 dBm. A dynamic range (defined as the range of linear dependence of the measured mode conversion efficiency over the RF drive power) of 25 dB was also measured.

In summary, we have realized, for the first time, an integrated MO Bragg cell module using a tapered structure in YIG-GGG waveguide. The curved hybrid lenses and lens pairs were shown to be capable of relatively large angular field of view at greatly reduced coma. The tapered waveguide structure was shown to be capable of satisfying simultaneously the requirements of large MO interaction bandwidth and high lens throughput. Optimization of device parameters should result in MO Bragg cell modules of improved performance. For example, a wider MO interaction bandwidth and thus a

larger number of resolvable scanned spots can be achieved by employing a thicker YIG layer in the middle region of the tapered waveguide and a microstrip transducer of smaller width than 60 μm. Also, a higher diffraction efficiency can be accomplished by utilizing a longer interaction length than 5.0 mm. The integrated MO Bragg cell modules should pave the way for realization of integrated MO circuits similar to the integrated AO circuits that have been realized most recently.

REFERENCES

[1] P.K. Tien and R.J. Martin, "Optical Waveguides of Crystal Garnet Films," Appl. Phys. Lett., Vol.21, pp.207-209, 1972.

[2] C.S. Tsai and D. Young, "Magnetostatic-Forward-Volume-Wave-Based Guided-wave Magneto-optic Bragg Cells and Applications to Communications and Signal Processing," IEEE Trans. Microwave Theory and Techniques, vol.38, pp.560-570, 1990.

[3] D. Young and C.S. Tsai, "GHz Bandwidth Magnetooptic Interaction in YIG-GGG Waveguide Using Magnetostatic Forward Volume Waves," Appl. Phys. Lett., vol.53, pp.1696-1698, 1988.

[4] D. Young and C.S. Tsai, "X-band Magnetooptic Bragg Cells Using Bismuth-doped Yttrium Iron Garnet Waveguides," Appl. Phys. Lett., vol.54, pp.2242-2244, 1989.

[5] T.Q. Vu, J.A. Norris, and C.S. Tsai, "Planar Waveguide Lenses in GaAs by Using Ion Milling," Appl. Phys. Lett., vol.54, pp.1098-1100, 1989.

[6] T.Q. Vu, J.A. Norris, and C.S. Tsai, "Formation of Negative Index-Change Waveguide Lenses in $LiNbO_3$ Using Ion Milling," Opt. Lett., vol.13, pp.1141-1143, 1988.

[7] T.Q. Vu, C.S. Tsai, D. Young, and C.L. Wang, "Ion-milled Lenses and Lens Arrays in Yttrium Iron Garnet-Gadolinium Gallium Garnet Waveguides," Appl. Phys. Lett., vol.55, pp.2271-2273, 1989.

[8] Y. Pu and C.S. Tsai, "RF Magnetization of Magnetostatic Forward Volume Wave in a YIG-GGG Layered Structure with Application to Design of High-Performance Guided-wave Magnetooptic Bragg Cell," International Journal of High Speed Electronics, vol.2, pp.185-208, 1991.

[9] E. Delano, "Primary Aberration of Menicus Fresnel Lenses," J. Opt. Soc. Am., vol.66, pp.1317-1320, 1976.

[10] C.L. Wang and C.S. Tsai, "High-Performance Curved Hybrid Lenses in YIG-GGG Waveguide," (to be published)

[11] C.L. Wang, Y. Pu and C.S. Tsai, "Permanent Magnet-Based Guided-Wave Magnetooptic Bragg Cell Modules," IEEE Journal of Lightwave Technology, vol.JLT-10, pp.644-648, 1992.

[12] See, for example, C.S. Tsai (Ed.), Guided-Wave Acousto-Optics, Springer Series in Electronics and Photonics, vol.23, 1990

[13] C.S. Tsai, "Integrated Acoustooptic Circuits and Applications," IEEE Trans. Ultrasonics, Ferroelectrics and Frequency Control, vol.39, No.4, 1992.

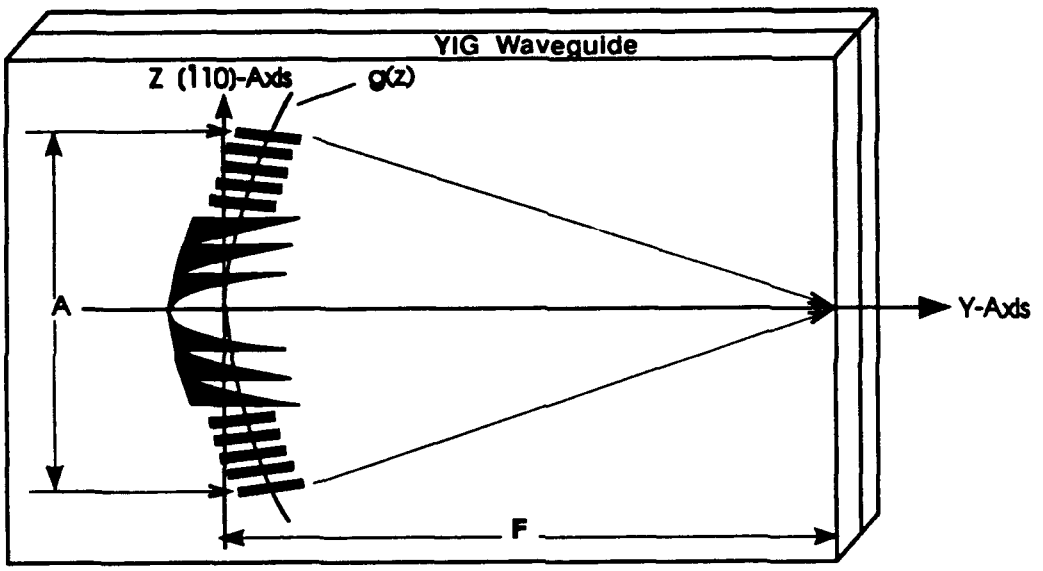

Fig.1: Curved Hybrid Lens on A YIG-GGG Waveguide

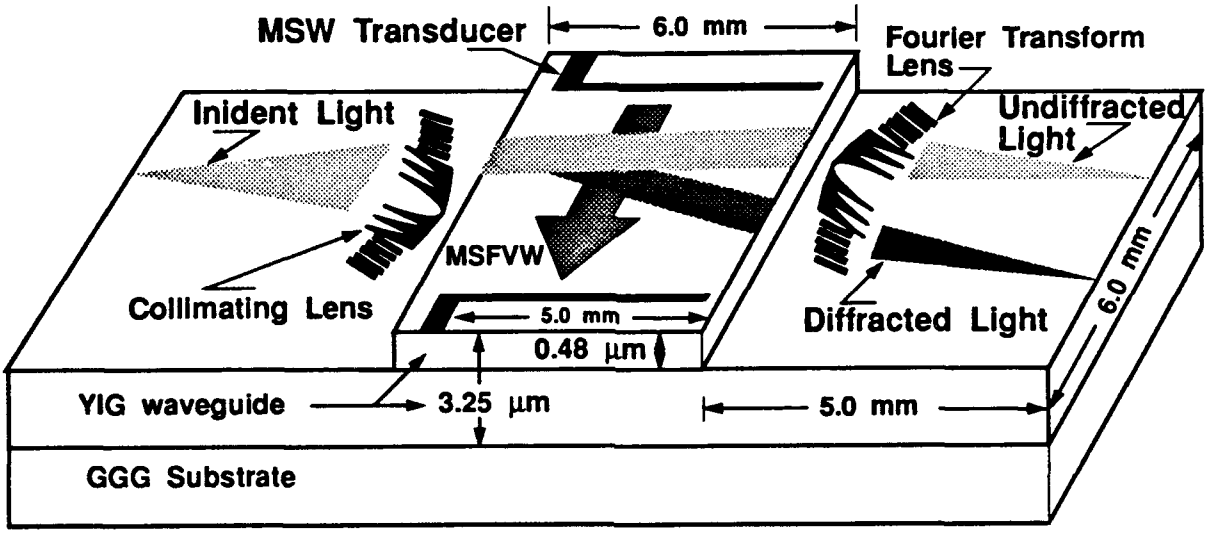

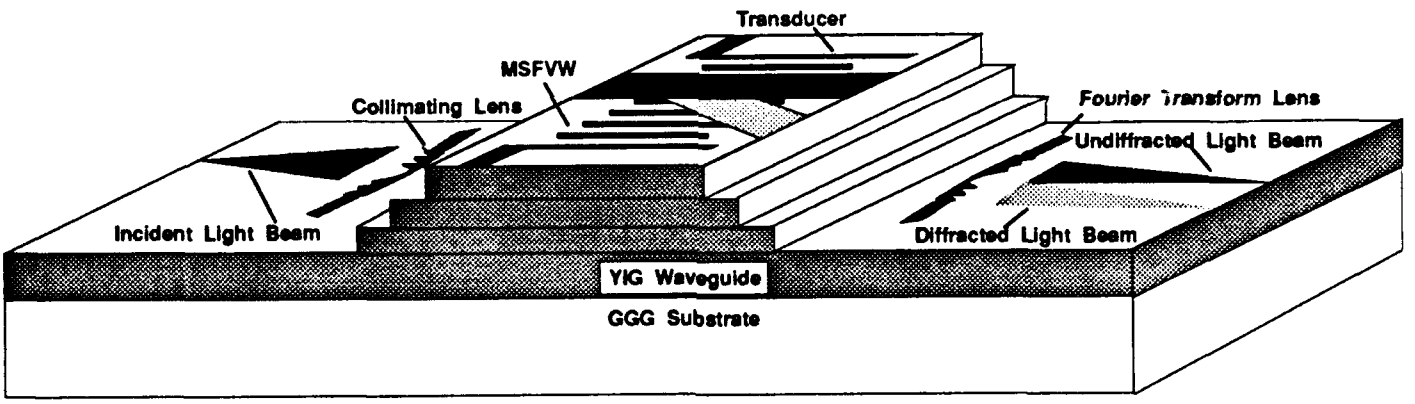

Fig.2: Integrated MO Bragg Cell Module on Bi-YIG-GGG Tapered Waveguide Structure

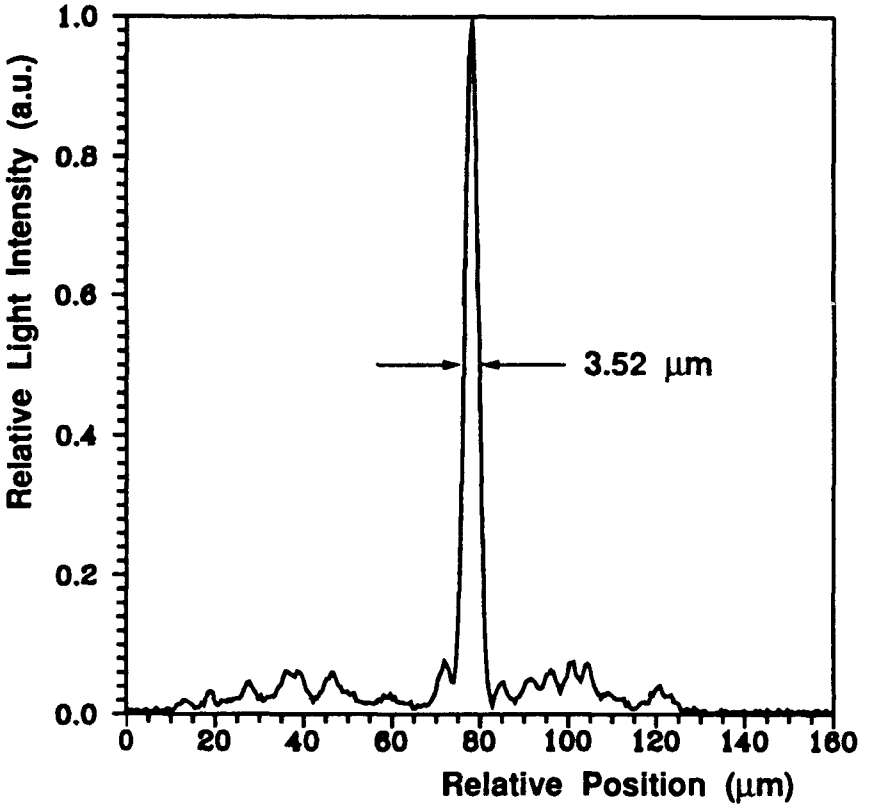

Fig.3(a): Measured Profile of Focused Light Spot from A Single Curved Hybrid Lens for Light Propagating along the Lens Axis

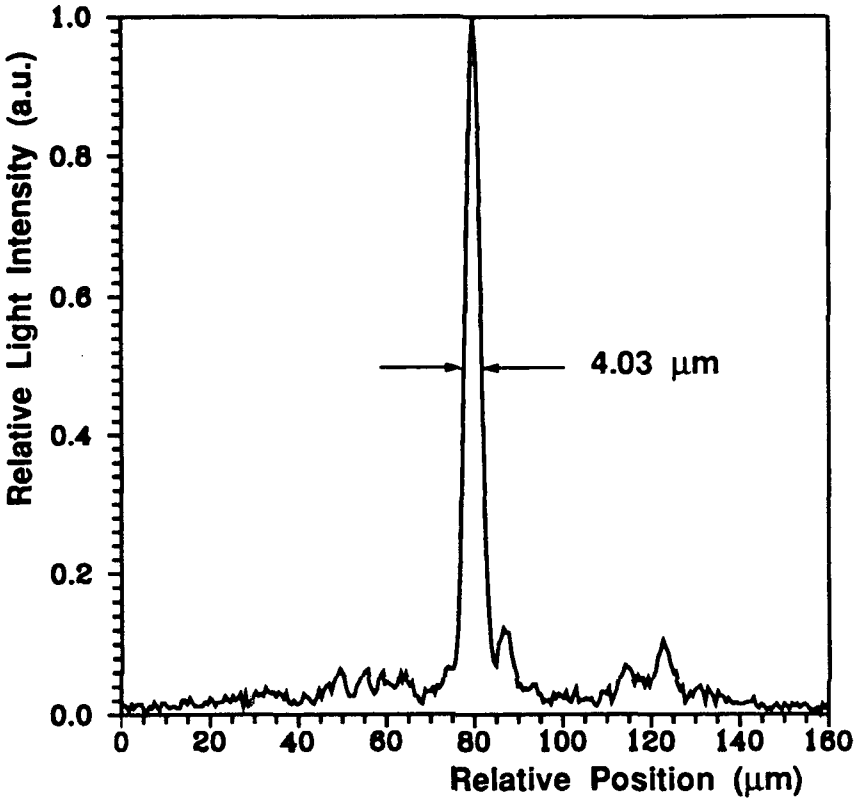

Fig.3(b): Measured Profile of Focused Light Spot from A Single Curved Hybrid Lens for Light Propagating at Oblique Angle of 3.5°

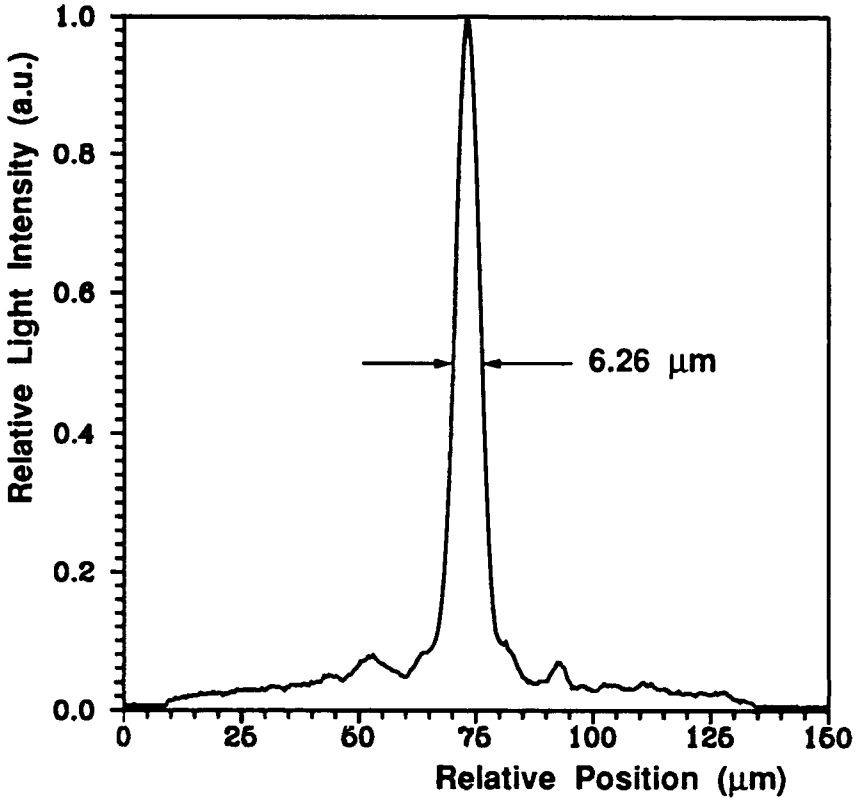

Fig.3(c): Measured Profile of Focused Light Spot from A Curved Hybrid Lens Pair for Light Propagating along the Lens Axis

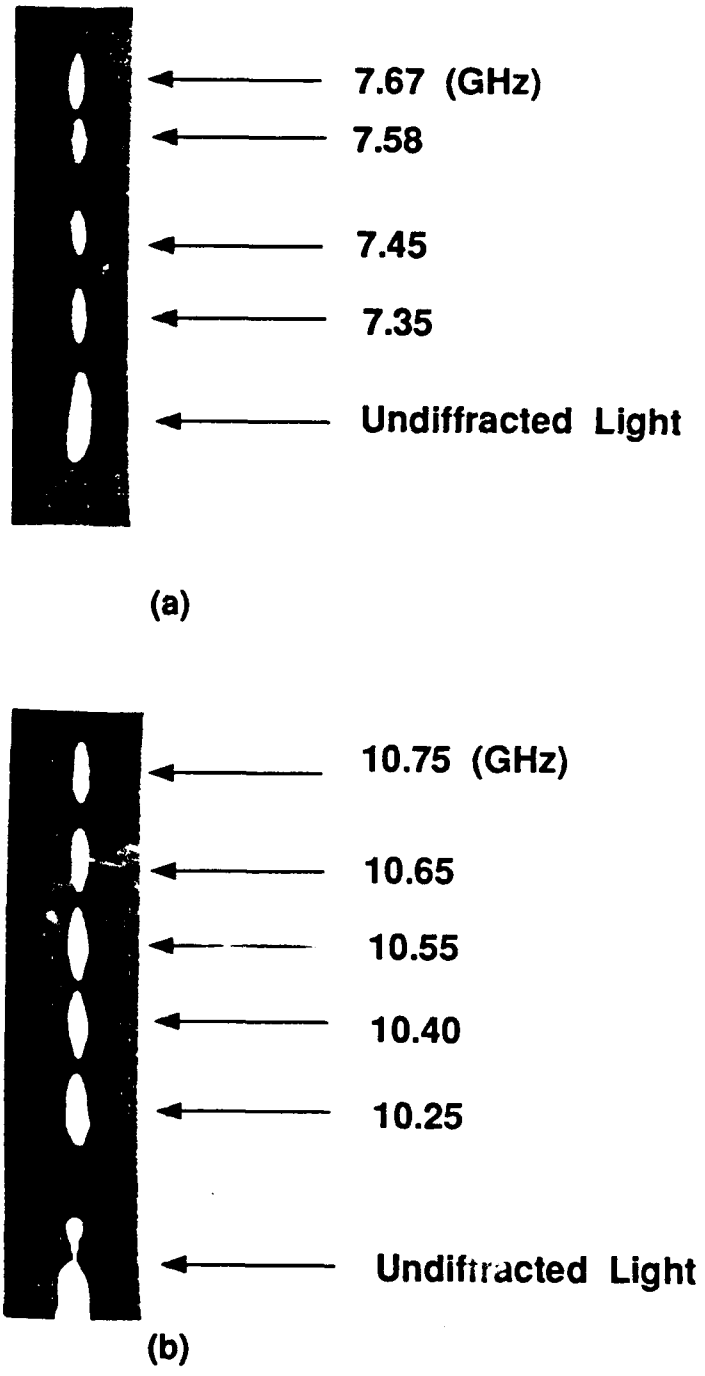

Fig.4: Scanned Focused Beam Spots of Diffracted Light versus Carrier Frequency Obtained by Integrated MO Bragg Cell Module at the DC Magnetic Field of (a) 2820 and (b) 3700 Oe

III. PUBLICATIONS RESULTING FROM ONR SUPPORT

1. Y. Pu and C.S. Tsai,"Magnetization of Magnetostatic Forward Volume Wave in a YIG-GGG Layered Structure with Application to Guided-Wave Magnetooptical Bragg Cell," Proc. of 1990 Ultrasonics Symposium, pp.213-216, IEEE Cat.#:90CH2938-9, ISSN:1051-0117.
2. Y. Pu, C.L. Wang, and C.S. Tsai,"High-Performance Magnetostatic Backward Volume Waves-Based Guided Wave Magnetooptic Bragg Cells with Application to Wide-Angle Light Beam Scanning," Integrated Photonics Research, 1991, Technical Digest Series (Optical Society of America, Washington, D.C. 1991), pp.20-21.
3. C.L. Wang, Y. Pu, and C.S. Tsai,"Compact Magnetostatic Wave-Based Magnetooptic 3Bragg Cell Module by Utilizing Small Permanent Magnet," Topical Meeting on Gradient-Index Optical Systems, 1991, Technical Digest Series (Optical Society of America, Washington, D.C.,1991),pp.74-77.
4. Y. Pu, C.L. Wang, and C.S. Tsai,"Magnetostatic Backward Volume Wave-Based Guided-Wave Magnetooptic Bragg Cells and Application to Wide-Band Light Beam Scanning," IEEE Photonics Technology Lett., Vol.3, pp.462-465, May 1991.
5. C.S. Tsai,"Guided-Wave Magnetooptic and Acoustooptic Bragg Cells for RF Signal Processing,"SPIE, Vol.1562, pp.55-65, July 1991, (Invited paper).
6. Y. Pu and C.S. Tsai,"RF Magnetization of Magnetostatic Forward Volume Wave in a YIG-GGG Layer Structure with Application to Design of High-Performance Guided-Wave Magnetooptic Bragg Cells," International Journal of High Speed Electronics, Vol.2, pp.185-208, Dec.1991 (Invited Paper).
7. Y. Pu and C.S. Tsai,"Noncollinear Magneto-optic Bragg Diffraction Using Magnetostatic Backward Volume Wave and Application to RF Spectral Analysis," Proc. of 1991 Ultrasonics Symposium, IEEE Cat.No.91CH3079-1, pp.205-209, Dec.8-11, Orlando, FL.

8. C.L. Wang and C.S. Tsai,"Guided-Wave Magnetooptic Bragg cell Modules using Compact Tunable Magnetic Housing," Proc. of 1991 Ultrasonics Symposium, IEEE Cat.No.91CH3079-1, pp.211-215, Dec.8-11, Orlando, FL.

9. C.L. Wang, Y. Pu and C.S. Tsai, "Permanent Magnet-Based Guided-Wave Magnetooptic Bragg Cell Modules," IEEE Journal of Lightwave Technology, vol.JLT-10, pp.644-648, May, 1992.

10. C.L. Wang, C.S. Tsai, and T. Ryuo,"Integrated Magneto-optic Bragg Cell Module in Tapered YIG-GGG Waveguide," 1992 Topical Meeting on Integrated Photonics Research, April 13-15, New Orleans, LA, 1992 Technical Digest Series, Vol.10, pp.98-99.

11. C.S. Tsai, Y. Pu, and C.L. Wang,"High-Performance Guided-Wave Magneto-optic Bragg Cells and Applications," Conference on Lasers and Electro-optics, 1992 Technical Digest Series, Vol.12, pp.514-517, May 10-15, Anaheim, CA.

IV. TECHNICAL PERSONNEL

Principal Investigator:

Dr. Chen S. Tsai

Ph.D. Research Assistants:

C.L. Wang (Expected to receive Ph.D. in Sept. 1992)

Y. Pu

Z.Y. Ren

V. TECHNICAL INTERACTIONS

1. Dr. Andy Yang of DARPA visited the group and observed the MO experiments on July 23, 1991.
2. Professor Jim Merz of UC Santa Barbara visited the group and observed the MO experiments on Feb.7, 1992.
3. Dr. O. Tamada of Sony Corp., Japan visited the group and observed the MO experiments on Feb.27, 1992. Dr. Tamada also brought us some YIG-GGG waveguide samples grown by SONY for measurement and characterization. Potential future cooperation was also discussed.
4. Dr. Bob Adler form Zenith Electronics Co., a world-renown scientist and engineer in Bulk-Wave Acoustooptics, visited the group on May.7-9, 1992, and provided valuable suggestions in connection with the magnetic circuits that facilitate miniaturization of the MO Bragg cell, and the electronic circuits for realization integrated MO frequency shifter modules.
5. Some 60 local industrial scientists and engineers visited the group and observed the MO experiments on May 8, 1992 during attendance and participation of the Research Review on Optical and Solid-State Devices.
6. Professor Richard Pantell, Director of Ginzton Microwave Laboratories of Stanford University, Professor S. Kawakami of Tohoku University in Japan, and Dr. Bob Montgomery, principal scientist of Harris Corp., visited the group on May 15,1992 and observed the MO experiments. Dr. Montgomery expressed interest in joint exploration of the MO Bragg cells for RF signal processing at X-band and beyond.